Exploiting Ambiguities in the Analysis of Cumulative Matching Curves for Person Re-identification

Vito Renò[1], Angelo Cardellicchio[2], Tiziano Politi[2], Cataldo Guaragnella[2] and Tiziana D'Orazio[1]
[1]*Institute of Intelligent Systems for Automation, Italian National Research Council, via Amendola 122 D/O, 70126 Bari, Italy*
[2]*Dipartimento di Ingegneria Elettrica e dell'Informazione, Politecnico di Bari, via Orabona 4, 70126 Bari, Italy*

Keywords: Person Re-Identification, Computer Vision, Video Surveillance.

Abstract: In this paper, a method to find, exploit and classify ambiguities in the results of a person re-identification (*PRID*) algorithm is presented. We start from the assumption that *ambiguity* is implicit in the classical formulation of the re-identification problem, as a specific individual may resemble one or more subjects by the color of dresses or the shape of the body. Therefore, we propose the introduction of the *AMbiguity rAte in RE-identification* (*AMARE*) approach, which relates the results of a classical PRID pipeline on a specific dataset with their effectiveness in re-identification terms, exploiting the ambiguity rate (AR). As a consequence, the cumulative matching curves (CMC) used to show the results of a PRID algorithm will be filtered according to the AR. The proposed method gives a different interpretation of the output of PRID algorithms, because the CMC curves are processed, split and studied separately. Real experiments demonstrate that the separation of the results is really helpful in order to better understand the capabilities of a PRID algorithm.

1 INTRODUCTION

One of the most interesting topics regarding the improvement of video surveillance systems is *person re-identification* (*PRID*), i.e. the re-identification of the same individual given two (or more) different views acquired by a set of non-overlapping cameras covering the same environment.

This task has become a crucial topic in the last few years, when the increased need for security originated from events like the September 11th has led to the deployment of a great number of video surveillance cameras over crowded areas like airports or train stations. As these cameras produce a large, and often hardly manageable, amount of raw video data, a way to properly analyze and classify them without the intervention of an human operator is needed.

The PRID task is complicated by a certain number of related problems, which can be divided in two categories (Saghafi et al., 2014):

- *Intra-camera Issues:* these issues are essentially related to the internal configuration of each camera, and may reguard the low resolution of the sensor, occlusion phenomena or different acquisition conditions;
- *Inter-camera Issues:* these issues are essentially related to the configuration of the camera set, in which each camera is subject to different lighting conditions and may have different hardware features.

The PRID methods proposed in literature try to deal with these issues, extracting relevant information from each view to properly characterize each individual. In order to do this, PRID methods use two kinds of feature:

- *Appearance:* these features are related to the appearance of the individual, and include *texture*, *color* and *shape* (Farenzena et al., 2010) (Gheissari et al., 2006) (Roy et al., 2012) (D'Orazio and Guaragnella, 2012);
- *Non-appearance:* these include features not related to the appearance of the individual, like*gait* (Bauml and Stiefelhagen, 2011).

Various datasets have been acquired in order to test the effectiveness of PRID methods (Bedagkar-Gala and Shah, 2014), each one differing from the others for the acquisition settings. Intuitively, not all datasets are well suited to test every PRID algorithm, as one dataset may present specific issues and advantage the use of certain features; thus, the application of the same algorithm to different datasets may give

Renò, V., Cardellicchio, A., Politi, T., Guaragnella, C. and D'Orazio, T.
Exploiting Ambiguities in the Analysis of Cumulative Matching Curves for Person Re-identification.
DOI: 10.5220/0005822104840494
In *Proceedings of the 5th International Conference on Pattern Recognition Applications and Methods (ICPRAM 2016)*, pages 484-494
ISBN: 978-989-758-173-1

inconsistent results.

In this work, we address this problem introducing the *Ambiguity Rate*, an index that relies the results given by a PRID algorithm with the specific dataset against which this algorithm is being tested. The main idea is to evaluate the statistical properties of the results given by the application of the PRID algorithm of the results of the PRID method: informally speaking, if an high variance is associated with these results, it may be reasonable to assume that the algorithm is not well suited to operate on that specific dataset; on the other side, if we obtain a low variance, the dataset is very ambiguous for these features, so the algorithm works properly.

The rest of this paper is structured as follows. In the second section, we formalize the basilar concept of the PRID task. In the third section, we expose our methodology, and we expose some results in the fourth section. In the fifth section, the conclusion and some perspectives on the future works are given.

2 MATHEMATICAL FORMULATION OF THE PRID TASK

2.1 PRID Task

Given a generic image dataset D which can be partitioned into a *gallery set* G and a *probe set* P, associate to each image of G the subset of the images of P which minimize a certain distance metric d.

Given c cameras, we hypothesize that each one of them acquire exactly one frame for each of the n individuals who pass through the video surveillance system, so:

$$|D| = n * c$$

As a consequence, in the most generic case:

$$D = G \cup P$$
$$|G| = n = N_G$$
$$|P| = n * (c-1) = N_P$$

Informally speaking, G contains *exactly* one view per individual, while P may contain one or more views per individual, according to the number of cameras.

The PRID task is generically ascribable to what we define as *PRID pipeline*, which is usually structured in three different steps. We hypothize that D has already been splitted in G and P.

Image Segmentation. In this phase each frame is subject to a pre-processing step, which includes *background subtraction* ((Stauffer and Grimson, 1999), (Zivkovic, 2004), (Jojic et al., 2009), (Renò et al., 2014),(Spagnolo et al., 2004)), *human detection* ((Dalal and Triggs, 2005), (Corvee et al., 2012)) and *shadow suppression* ((Lu and Zhang, 2007)), in order to discard noisy information reguarding background and shadows.

Descriptor Extraction. In this phase a robust and discriminative descriptor is computed per each frame combining both texture and chromatic features.

Descriptor Matching. In this phase the descriptor of the each image belonging to G is compared with the descriptors of the images belonging to P, searching for the best match (i.e. the one which minimize the distance metric d).

Over the years, various approaches to the different phases of the PRID pipeline have been proposed. The proposed methods can be classified in three ways.

2.1.1 Appearance vs. Non-appearance Methods

We can discriminate the PRID algorithm basing on the kind of features used to extract the frame descriptor, as stated in the first section.

2.1.2 Single-shot vs. Multiple-shot Methods

We can discriminate the single-shot case from the multiple-shot case evaluating both the cardinality of G and P and the number of frames used to extract a descriptor for the appearance of each individual.

In the single-shot case, the descriptor S_i of the i-th individual is computed as:

$$|G| = |P|$$
$$\forall i \in D : \begin{cases} S_{G_i} = g(f_{G_i}) \\ S_{P_i} = g(f_{P_i}) \end{cases}$$

More informally, the cardinality of both the gallery set and the probe set is equal to n, as there are only two cameras which acquire exactly one view per individual. As a consequence, for each individual in G the signature S_{G_i} is a generic function $g(\cdot)$ of the unique frame f_G related to the individual i, and this is true also for the corresponding signature S_{P_i} extracted from the frame f_P which depicts the individual in the probe set.

The multiple-shot case is slightly different:

$$|G| < |P|$$
$$\forall i \in D : \begin{cases} S_{G_i} = g(f_{G_i}) \\ S_{P_i} = h(f_{P_{1,i}}, \ldots, f_{P_{c,i}}) \end{cases}$$

We note that the cardinality of G is *strictly* less than the cardinality of P. It means that the function

$g(\cdot)$ used to extract S_{G_i} cannot be used to compute S_{P_i}, as it has to be modified to take in account c parameters, i.e. the f_{P_j} frames related to the i-th individual, with $j = 1, ..., c$. We denote the modified function used to extract S_{P_i} with $h(\cdot)$.

Obviously, multiple-shot methods may provide a richer and more discriminative descriptor than single-shot methods, meaning that the PRID task is easier in the multiple-shot case. A review about single-shot and multiple-shot methods is given in (D'Orazio and Cicirelli, 2012).

2.1.3 Contextual vs. Non-contextual Methods

Contextual PRID methods are strictly dependent on the context of the video surveillance system. There are two types of contextual PRID methods:

- *Camera Geometry Methods:* these methods exploit the spatial and temporal relationships between cameras in the dataset (Javed et al., 2008);
- *Camera Calibration:* these methods exploit camera calibration or homography tecniques to extract discriminative descriptor for PRID purposes (Lantagne et al., 2003).

Non-Contextual methods do not use context information, and may be distinguished into *passive* methods, which do not rely on learning techniques for descriptor matching, and *active* methods, which employ supervised or unsupervised learning algorithms for descriptor extraction or matching (Bedagkar-Gala and Shah, 2014). Active methods can be further classified into:

- *Color Calibration Methods:* these methods exploit color calibration techniques to model chromatic relationships between cameras in a given camera set. Usually, a *brightness transfer function* (*BTF*) (D'Orazio et al., 2009) is learned between each pair of cameras in a training stage and used to improve PRID robustness;
- *Descriptor Learning Methods:* these methods evaluate the various features used to compute the descriptor of each frame and choose the most meaningful ones or at least a discriminative weighting scheme to apply to a raw feature vector in order to extract a robust descriptor (Zheng et al., 2009; Wang et al., 2007; Gray and Tao, 2008);
- *Distance Metric Learning Methods:* these methods attempt to maximize the matching accuracy between frame descriptors, employing a training stage where a distance metric is learned throught the resolution of a convex programming problem which allows to evaluate a symmetric positive-semidefinite matrix D that will be used in a quadratic distance framework. A comprehensive survey on these approaches is given in (Yang and Jin, 2006).

Finally, the results are displayed on the Cumulative Matching Characteristic (CMC) curve, that represents the expectation of finding the correct match in the top n matches of the chosen algorithm ((Farenzena et al., 2010)). More specifically, the x axis of such curve represents the rank and the y one the percentage of recognition (or the number of images recognized). For example, a CMC value of 50% for a rank r means that the 50% of the images taken from the gallery set can be found in a range of ranks between 1 and r, because of the cumulative nature of the curve. An example of CMC is shown in Figure 2(a) and 2(b).

3 METHODOLOGY

3.1 Algorithm Description

The proposed algorithm, named *AMARE*, is divided in three main steps, as it is shown in figure 1:

1. Ambiguity Descriptor calculation (in blue);
2. Ambiguity evaluation (in red);
3. CMC separation (in green).

The first step takes place in a *preprocessing phase*, while the other two need to be executed in a *postprocessing stage*. This means that *the PRID pipeline is enriched by two modules that aim to quantify the accuracy of a generic re-identification algorithm*. Attention will also be focused on the computational complexity of the whole approach, as it is pointed out in the corresponding subsection.

3.1.1 Ambiguity Descriptor Calculation

Given a generic dataset D, an *Ambiguity Descriptor* (*ad*) is calculated for each frame. The *ad* is an arbitrary-rank tensor that embeds information about the kind of scene that is being observed, allowing heterogeneous features to be exploited in order to define this kind of descriptor.

Nevertheless, we start from the assumption that an operator who is manually supervising a surveillance system will probably try to estimate the accuracy of the results with respect to the color of the images returned by the algorithm.

We follow the framework defined in (Cardellicchio et al., 2015), using an ambiguity descriptor which takes in account the tint of an image preserving spatial information about the location of the specific colour. Therefore, we divide the i-th frame of D in six horizontal stripes and then calculate the trend value of the Hue coordinate for each stripe, assuming that the images are in the HSV format. Hence, the ad is a six elements vector of natural numbers:

$$ad_i = \begin{pmatrix} \tau_1 \\ \vdots \\ \tau_6 \end{pmatrix} \in \mathbb{N}^6 \qquad (1)$$

$$\forall i \in D$$

3.1.2 Ambiguity Evaluation

Given a set of q PRID algorithms to test

$$ALG = \{\alpha_1, \alpha_2, \ldots, \alpha_q\} \qquad (2)$$

the best M results of each algorithm α_i are stored in a matrix R_{α_i} while the respective ranks are stored in a column vector K_{α_i}

$$K_{\alpha_i} = \begin{pmatrix} k_1 \\ k_2 \\ \vdots \\ k_{N_G} \end{pmatrix} \in \mathbb{N}^{N_G} \qquad (3)$$

$$R_{\alpha_i} = \begin{pmatrix} r_{11} & r_{12} & \ldots & r_{1M} \\ r_{21} & r_{22} & \ldots & r_{2M} \\ \vdots & \vdots & \vdots & \vdots \\ r_{N_G 1} & r_{N_G 2} & \ldots & r_{N_G M} \end{pmatrix} \in \mathbb{N}^{(N_G \times M)} \qquad (4)$$

In the matrix there is one row for each image taken from the gallery set G and the results are ordered by descendant score of the specific algorithm within each row. Since an r_{ij} element is an image taken by the probe set P with an ambiguity descriptor $ad_{r_{ij}}$ associated to it, also these descriptors can be stored in an Ambiguity Descriptor Matrix $ADM_{\alpha_i} \in \mathbb{N}^{(N_G \times M)}$ that has the same structure of the previous one. Consequently, each element must be replaced by the descriptor chosen in the preprocessing stage and exploited in order to obtain the Ambiguity Rate (AR). In this work, the z-th row of ADM_{α_i} is a matrix

$$ADM^z_{\alpha_i} = \left(ad_{r_{z1}}, ad_{r_{z2}}, \ldots, ad_{r_{zM}}\right) =$$
$$= \begin{pmatrix} \tau_{11} & \tau_{12} & \ldots & \tau_{1M} \\ \tau_{21} & \tau_{22} & \ldots & \tau_{2M} \\ \vdots & \vdots & \vdots & \vdots \\ \tau_{61} & \tau_{62} & \ldots & \tau_{6M} \end{pmatrix} = \begin{pmatrix} \tau S^T_1 \\ \tau S^T_2 \\ \vdots \\ \tau S^T_6 \end{pmatrix} \qquad (5)$$

where τS^T_i is the row vector that contains the trend values of the M best frames with respect to the i-th stripe. Such rows are used to calculate the percentage deviation ($\%_\tau$) of the trend values while preserving the spacial information about the Hue value using the following formula:

$$\%^z_\tau = \begin{pmatrix} \frac{\max(\tau S^T_1) - \min(\tau S^T_1)}{256} \\ \vdots \\ \frac{\max(\tau S^T_6) - \min(\tau S^T_6)}{256} \end{pmatrix} \qquad (6)$$

Finally, the AR value is calculated as the average value of the percentage deviations

$$AR^z_{\alpha_i} = 1 - \frac{1}{6} \sum_{s=1}^{6} \%^z_\tau(s) \qquad (7)$$

so that an high variation of the percentual displacement returns no ambiguity. This index is ready to be used to correct the results of the CMC curve. This task is described in the next subsection.

3.1.3 CMC Separation

The CMC curve is calculated as described in the previous paragraph using only the information about the ranks (equation 3). The aim of this work is to split this curve evaluating its building blocks, and this operation can be achieved with the fuzzification of the ranks according to the AR value in the following way:

$$[0, 0.4] \Rightarrow LOW$$
$$(0.4, 0.9] \Rightarrow MEDIUM$$
$$(0.9, 1] \Rightarrow HIGH$$

Therefore, the CMC curves can be calculated again considering three different contributions that reflect the three levels of the ambiguity rate.

3.2 Computational Complexity

The computational complexity of this approach is strictly dependent on the parameters used to model the ambiguities. The number of operations may significantly vary according to the descriptor chosen, as it can be any n-dimensional tensor. Let $N_D = (N_G + N_P)$ be the cardinality of the dataset that is being processed, N_{px} the number of pixels and $f(\cdot)$ the number of operations required by the task, the computational complexities are the following:

1. **Ambiguity Descriptor Calculation** requires $O(k \cdot N_{px} \cdot N_D)$ operations to be processed, where
$$k = \sum_{i=1}^{K} f(i)$$
is the sum of the number of operations needed to calculate each element of the descriptor and K represents the dimensionality of the descriptor.

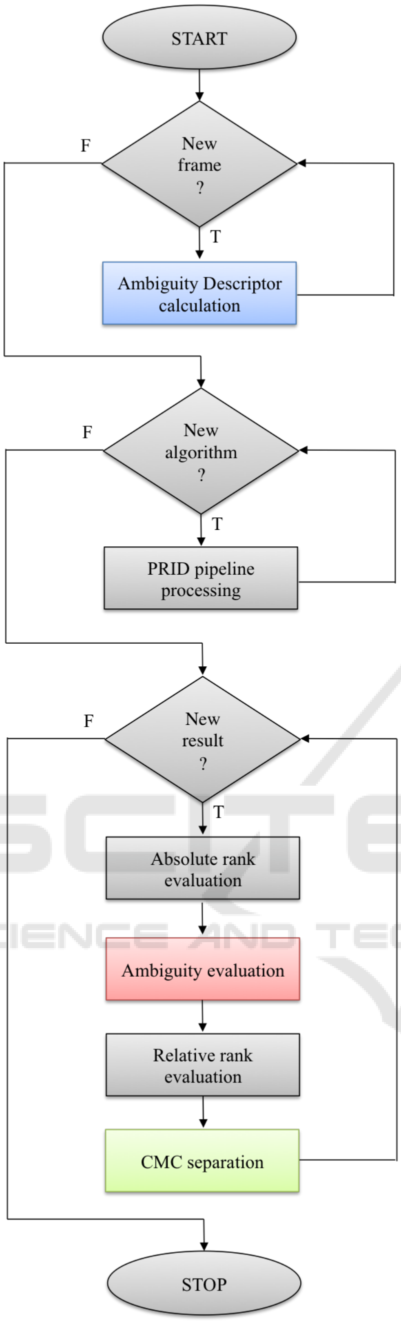

Figure 1: Algorithm high level flowchart.

2. **Ambiguity Evaluation** has a complexity of $O(q \cdot M \cdot N_D)$

Finally, the computational complexity of the ambiguity rate process computation depends on N_D, while the one of the whole process depends on the computational complexity of the most expensive algorithm.

4 EXPERIMENTS AND RESULTS

The methodology described in this paper has been tested on the PRID algorithms proposed in (Farenzena et al., 2010) and (Cardellicchio et al., 2015), in order to better understand the performances obtained on the dataset VIPeR (Gray et al., 2007). This dataset contains 632 images taken from non overlapping cameras with arbitrary viewpoints. All the images have been taken under varying illumination conditions and each one is scaled to 128×48 pixels. In (Farenzena et al., 2010), the authors use both color (MSCR and wHSV) and texture (RHSP) features to recognize the subjects, while in (Cardellicchio et al., 2015) only the color is exploited (HSV and *log* RG). However, the approach presented in this paper is focused on the interpretation of the results with respect to the CMCs.

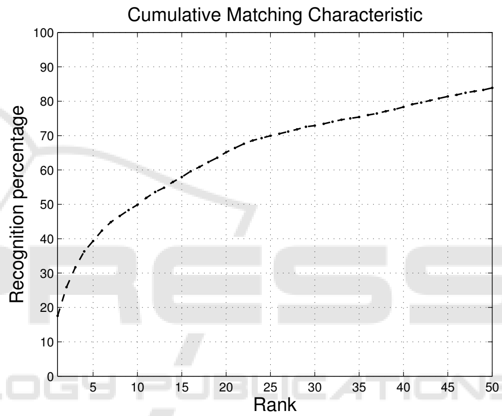

(a) Overall CMC - Algorithm (Farenzena et al., 2010)

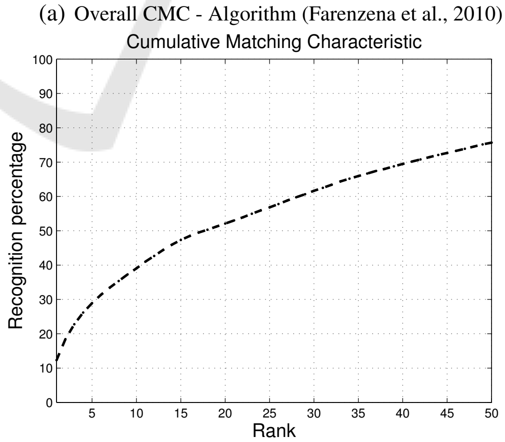

(b) Overall CMC - Algorithm (Cardellicchio et al., 2015)

Figure 2.

Figures 2(a) and 2(b) report the overall CMC that represent the state of art method used to measure the performances of the algorithms on the chosen dataset. Looking at the curves, algorithm (Farenzena et al., 2010) works better than the other because the

Figure 3: Results given by the traditional PRID pipeline. Visual matching for algorithm (Cardellicchio et al., 2015). The first column GS represents the query images taken from the Gallery Set, the second one contains the Foreground Masks, while the other columns are the responses taken from the Probe Set, ordered by the rank. The red box indicates the Ground Truth.

CMC starts from a higher value at the first rank and the values of the other ranks are always higher than the ones of algorithm (Cardellicchio et al., 2015). However, this curves present some drawbacks because they effectively embed information about the re-identification rank, but we actually don't know if the results for a specific rank have been obtained in ambiguous situations or not. For example, given the first rank, it is not possible to determine if the re-identification percentage has been achieved in *easy* or *hard* configurations. In fact, one would suppose that in cases of low ambiguity, the correct result should be returned at the first iteration. On the contrary, worst responses should be expected when the algorithm has to choose among ambiguous observations. Furthermore, figure 3 gives a graphical overview of a certain number of results. In this example, the first six images are correctly recognized by the algorithm because the first response is the one surrounded by the red box that represents the ground truth, i.e. the right image taken from the probe set that depicts the same subject of the query image. Rows from 7 to 10 show that the algorithm is giving a rank 2 response, while the last two represent a failure because there is no recognition in the first 20 responses. Looking at the images, it is possible to notice that there is no regularity in the responses with respect to the ambiguity. For example, in the second row there is a person with a green sweater, but the other images returned by the algorithm are really different one from the other. For this reason, the experiments presented in this section will exploit the AR value to understand how a specific algorithm is working given a specific ambiguity range.

First, the ambiguity descriptor is calculated according to equation 1 for each image of the collection. Then, the rest of the PRID pipeline is executed for both algorithms and finally the results are processed in order to calculate the ambiguity rate as described in equation 7. In order to obtain a visual comparison of the least ambiguous result and the most ambiguous one, an example of boxplot enriched by the corresponding frames is provided in figure 5 and 6. Each box refers to one of the stripes used to divide the images, as noticeable in the figure, so it is representative of one row of the ADM described in equation 5. Moreover, there is a blue circle that indicates the value of the ambiguity descriptor of the gallery set image, i.e. the one that is being re-identified by the algorithm. If the image taken from the gallery set is re-identified correctly, the blue circle should lie inside the box. Otherwise, the distance of the circle from the box can be exploited to understand how far the im-

Table 1: Dataset separation for different values of the ambiguity rate.

Ambiguity rate	(Farenzena et al., 2010)		(Cardellicchio et al., 2015)	
LOW	46 img	7.28 %	18 img	2.85 %
MEDIUM	559 img	88.45 %	581 img	91.93 %
HIGH	27 img	4.27 %	33 img	5.22 %

age is from the results, and so quantify how much an algorithm is doing wrong in a specific situation. In the first case (figures 5(a) and 5(b)) the situation is so ambiguous that each person can easily be misinterpreted even by an expert human operator because everyone wears similar clothes. In the second case (figures 6(a) and 6(b)), the images of the probe set are not so ambiguous, in fact the first 5 returned values are different one from the other: different colours of the shirt/dress (red, black, white and yellow) and different colours of the trousers/skirt (pink, black, red, jeans). Hence, a boxplot with large boxes will refer to a non ambiguous response, that should basically imply that the algorithm is operating in an *easy condition*, so the correct response should be given at the first rank. On the contrary, small boxes are related to ambiguous responses that are likely to be mistaken. In this situation, a good PRID algorithm answers with the correct image in one of the first ranks, but not always at rank 1.

Figure 4 shows the ambiguity rate histogram for each response of the two algorithms. It is immediate to notice that a small number of responses has a corresponding *LOW* ambiguity rate (< 0.4) or a *HIGH* one (> 0.9), according to the fuzzification rule presented in section 3.1.3.

Looking at Table 1, both algorithms are isolating about 10% of the images in the tails of the distribution, namely the 5% of the results of the algorithms has low ambiguity and similarly another 5% has high ambiguity. Looking at the peak of the distribution we observe that it is located around 0.6 for algorithm (Farenzena et al., 2010), that means that a medium level of ambiguity is produced most of the time. For algorithm (Cardellicchio et al., 2015), the peak is located around 0.7, that means that the responses are more similar one to the other. The corresponding CMC curves for *LOW*, *MEDIUM* and *HIGH* ambiguity rate values are reported in figure 7, 8 and 9 and are called *split CMC*. For each curve, the x axis reports the first 100 ranks and the y axis shows the percentage of images that have been recognized at the specific rank. Due to the cumulative nature of the curve, if there is a step, it means that there are no matches at the corresponding rank. For example, the CMC in figure 7(b) illustrates that algorithm (Cardellicchio et al., 2015) does not have any match at ranks

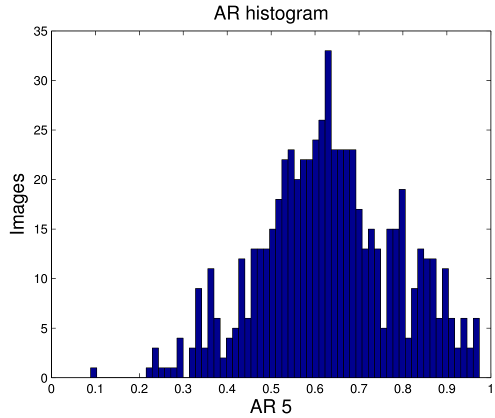

(a) Ambiguity rate distribution for algorithm (Farenzena et al., 2010). The peak is located around $AR = 0.6$.

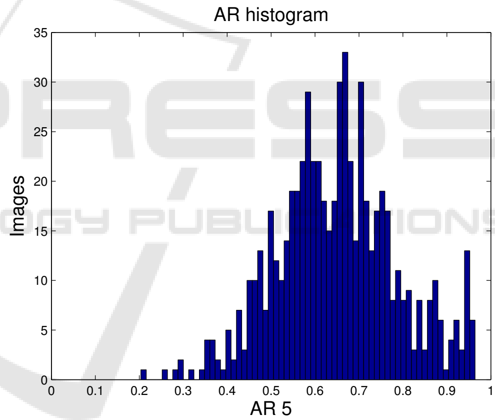

(b) Ambiguity rate distribution for algorithm (Cardellicchio et al., 2015). The peak is located around $AR = 0.7$.

Figure 4: Ambiguity rate histogram on VIPeR results.

$2, 3, 5-7, 9-19, 21-70\dots$, while the one in figure 7(a) is more similar to a curve, even if in some points it is flat (e.g. ranks $4, 5, 10-15\dots$). Here, algorithm (Cardellicchio et al., 2015) shows a high percentage than the other approach at rank 1. Such situation should be the easiest for an algorithm, so the expected result would be a really high percentage at rank 1.

The CMCs in figure 8(a) and 8(b) are similar to the ones already known in literature because they are representative of about 90% of the dataset. The last two curves indicate the response in *HIGH* ambiguity cases. In both cases (figure 9(a) and 9(b)) there is an increment of the correct answers starting from

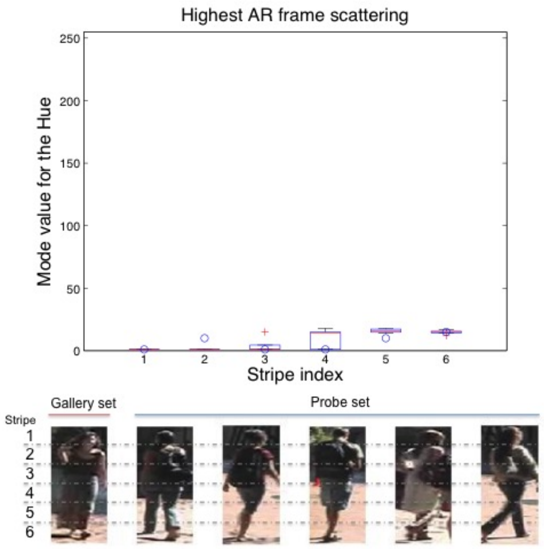

(a) Highest AR obtained with algorithm (Farenzena et al., 2010). The visual matching represents the query image (gallery set) and the first 5 responses. The boxes are referred to the probe set, while the circle represents the query.

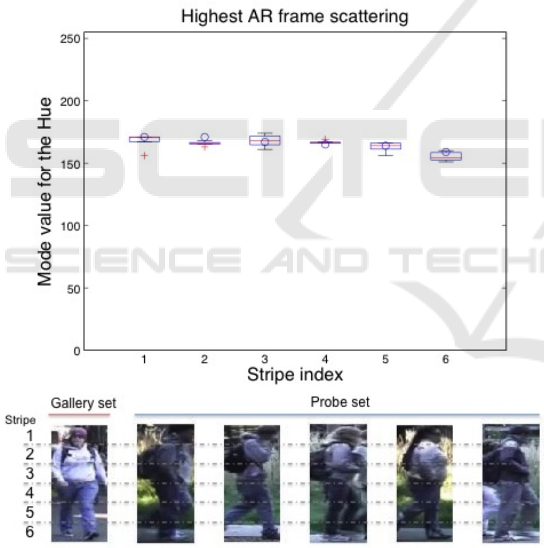

(b) Highest AR obtained with algorithm (Cardellicchio et al., 2015). The visual matching represents the query image (gallery set) and the first 5 responses. The boxes are referred to the probe set, while the circle represents the query.

Figure 5: Boxplot comparison for the highest AR and visual matching of the result.

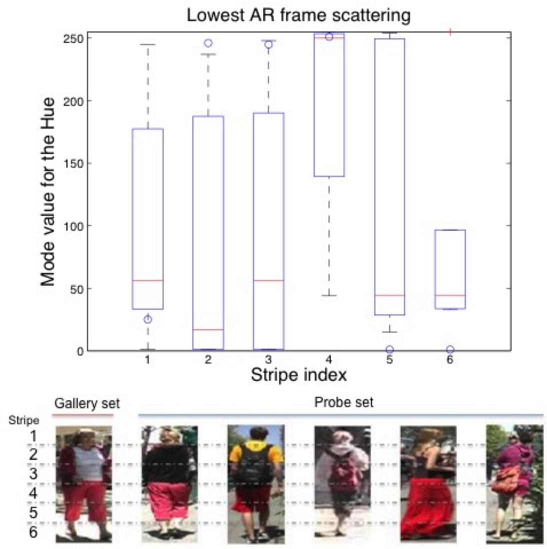

(a) Lowest AR obtained with algorithm (Farenzena et al., 2010). The visual matching represents the query image (gallery set) and the first 5 responses. The boxes are referred to the probe set, while the circle represents the query.

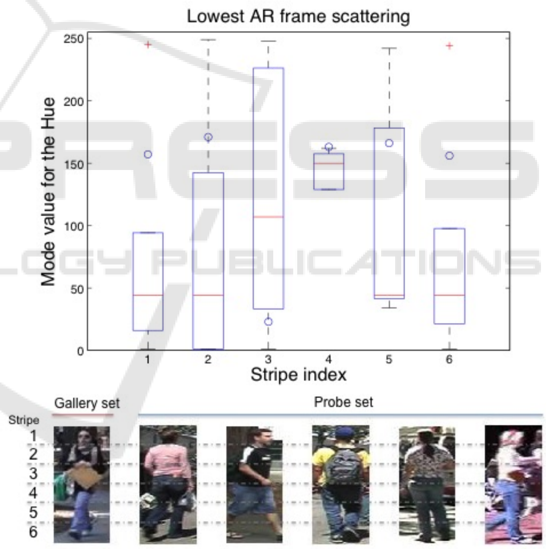

(b) Lowest AR obtained with algorithm (Cardellicchio et al., 2015). The visual matching represents the query image (gallery set) and the first 5 responses. The boxes are referred to the probe set, while the circle represents the query.

Figure 6: Boxplot comparison for the lowest AR and visual matching of the result.

rank 5. This is an interesting result because it means that both approaches do not give meaningful answers in the first iterations when operating in challenging situations. Focusing on low ranks, we notice that the algorithms give similar results for both *LOW* and *MEDIUM* ambiguity values. However, we expected that the majority of the low rank responses occurred in the condition $AR < 0.4$, thus obtaining the best results in *easy* configurations, i.e. when the images returned are really different one from the other. Finally, an algorithm should be able to increase the number of images that lie in *LOW* or *HIGH* ambiguity values. In the first case the recognition percentage at rank 1 should be the highest, while in the second one the correct response is expected within the first ranks. These quite uniform results for each ambiguity value

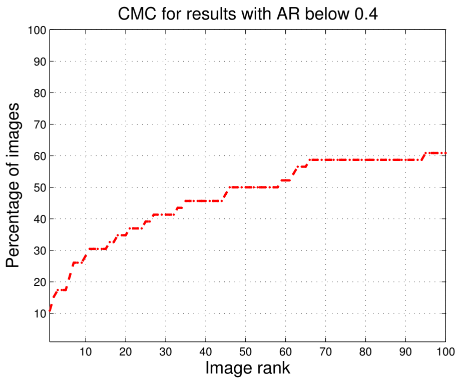

(a) CMC referred to the low ambiguity results obtained with algorithm (Farenzena et al., 2010). The cardinality of this set is 46 images.

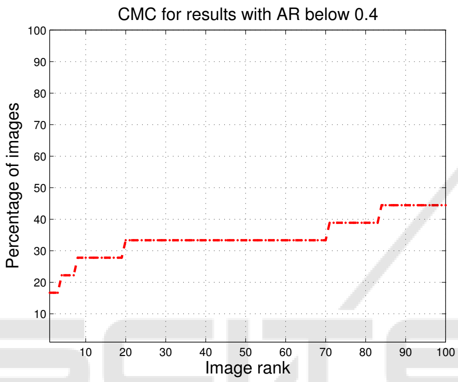

(b) CMC referred to the low ambiguity results obtained with algorithm (Cardellicchio et al., 2015). The cardinality of this set is 18 images.

Figure 7: CMC split comparison, LOW ambiguity values.

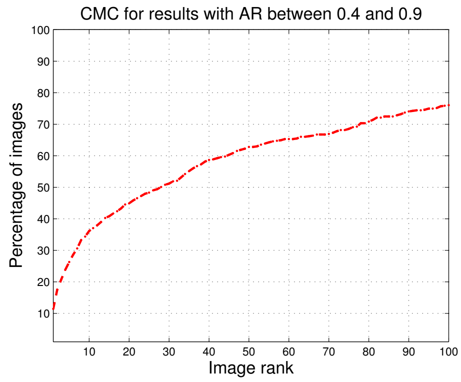

(a) CMC referred to the medium ambiguity results obtained with algorithm (Farenzena et al., 2010). The cardinality of this set is 559 images.

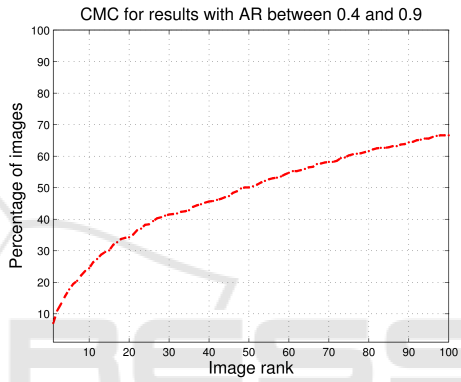

(b) CMC referred to the medium ambiguity results obtained with algorithm (Cardellicchio et al., 2015). The cardinality of this set is 581 images.

Figure 8: CMC split comparison, MEDIUM ambiguity values.

show how the features used by the algorithms can not isolate easy recognizable situations for a human eye. This is probably due to the representation of the colors in different visual systems: the human one and the digital one. For the first, peaks on different color tones can be immediately distinguishable, while in a digital color space the same peaks can generate values that are likely to be classified as similar colors even if they are different.

5 CONCLUSION

In this paper, a method to quantify the accuracy of a re-identification algorithm exploiting the ambiguity of its responses has been presented. This method enriches the PRID pipeline defining an ambiguity descriptor and taking advantage of it to calculate the AR of each response of the algorithm. This ambiguity can be seen as a *relative* one, because its formulation is dependent on the results of the chosen algorithm, as stated in equation 7 and it can be used to understand the operative conditions in which the algorithm works. Looking at the results presented in section 4, the performances of a generic algorithm can be studied exploiting its behaviour in ambiguous and non ambiguous situations. Moreover, the AR histogram (figure 4) gives an immediate graphical description of the ambiguity distribution among the images of a specific dataset. Finally, the split CMC curves can be studied separately using this information to measure the performance of different algorithms that run on the same dataset. In conclusion, the work presented in this paper can be seen as the first step in the exploitation of ambiguities in order to understand the results of a PRID pipeline. Future research trends will regard the extension of this approach in order to model an *absolute* ambiguity value associated to a dataset. Exploiting both *relative* and *absolute* ambiguities, a generic rank of a CMC can be promoted or penalized starting from the assumption that if an algorithm gives for example a rank 3 output in an ambiguous

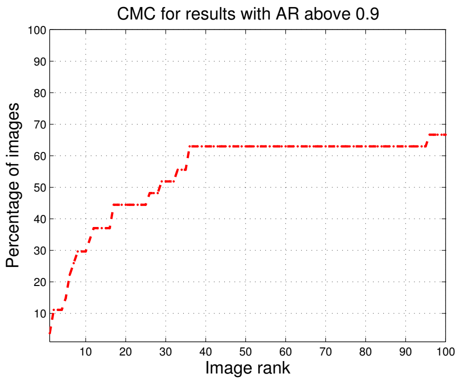

(a) CMC referred to the high ambiguity results obtained with algorithm (Farenzena et al., 2010). The cardinality of this set is 27 images.

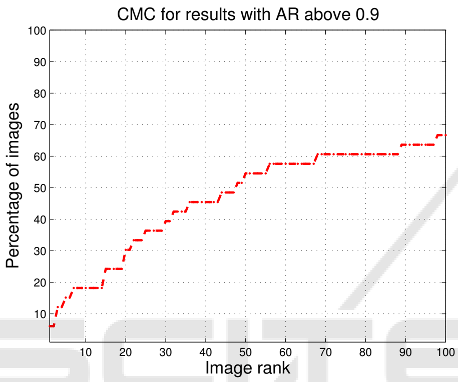

(b) CMC referred to the high ambiguity results obtained with algorithm (Cardellicchio et al., 2015). The cardinality of this set is 33 images.

Figure 9: CMC split comparison, HIGH ambiguity values.

situation, then it can be promoted. Moreover, if an algorithm does not give a rank 1 output in unambiguous situations (e.g. the re-identification of the only one person dressed with dark clothes in a controlled environment), then it can be penalized. Finally, the research on the *absolute* ambiguity value should give to an operator the possibility to compare different algorithms that run on different datasets.

ACKNOWLEDGEMENTS

The authors would like to thank Mr. Michele Attolico for his technical support.

REFERENCES

Bauml, M. and Stiefelhagen, R. (2011). Evaluation of local features for person re-identification in image sequences. In *Adv. Video and Signal-Based Surveill. (AVSS), 2011 8th IEEE Int. Conf. on*, pages 291–296. IEEE.

Bedagkar-Gala, A. and Shah, S. K. (2014). A survey of approaches and trends in person re-identification. *Image and Vis. Comput.*, 32(4):270–286.

Cardellicchio, A., D'Orazio, T., Politi, T., and Renò, V. (2015). An human perceptive model for person re-identification. In *VISAPP-Int. Conf. on Comput. Vis. Theory and Appl.-2015*.

Corvee, E., Bak, S., Bremond, F., et al. (2012). People detection and re-identification for multi surveillance cameras. In *VISAPP-Int. Conf. on Comput. Vis. Theory and Appl.-2012*.

Dalal, N. and Triggs, B. (2005). Histograms of oriented gradients for human detection. In *Comput. Vis. and Pattern Recognit., 2005. CVPR 2005. IEEE Comput. Soc. Conf. on*, volume 1, pages 886–893. IEEE.

D'Orazio, T. and Cicirelli, G. (2012). People re-identification and tracking from multiple cameras: A review. In *Image Process. (ICIP), 2012 19th IEEE Int. Conf. on*, pages 1601–1604.

D'Orazio, T. and Guaragnella, C. (2012). A graph-based signature generation for people re-identification in a multi-camera surveillance system. In *VISAPP*, volume 1, pages 414–417.

D'Orazio, T., Mazzeo, P., and Spagnolo, P. (2009). Color brightness transfer function evaluation for non overlapping multi camera tracking. In *Distrib. Smart Cameras, 2009. ICDSC 2009. Third ACM/IEEE Int. Conf. on*, pages 1–6. IEEE.

Farenzena, M., Bazzani, L., Perina, A., Murino, V., and Cristani, M. (2010). Person re-identification by symmetry-driven accumulation of local features. In *Comput. Vis. and Pattern Recognit. (CVPR), 2010 IEEE Conf. on*, pages 2360–2367. IEEE.

Gheissari, N., Sebastian, T. B., and Hartley, R. (2006). Person reidentification using spatiotemporal appearance. In *Comput. Vis. and Pattern Recognit., 2006 IEEE Comput. Soc. Conf. on*, volume 2, pages 1528–1535. IEEE.

Gray, D., Brennan, S., and Tao, H. (2007). Evaluating appearance models for recognition, reacquisition, and tracking. In *Proc. IEEE Int. Workshop on Perform. Eval. for Track. and Surveill. (PETS)*, volume 3. Citeseer.

Gray, D. and Tao, H. (2008). Viewpoint invariant pedestrian recognition with an ensemble of localized features. In *Comput. Vis.–ECCV 2008*, pages 262–275. Springer.

Javed, O., Shafique, K., Rasheed, Z., and Shah, M. (2008). Modeling inter-camera space–time and appearance relationships for tracking across non-overlapping views. *Comput. Vis. and Image Understanding*, 109(2):146–162.

Jojic, N., Perina, A., Cristani, M., Murino, V., and Frey, B. (2009). Stel component analysis: Modeling spatial correlations in image class structure. In *Comput. Vis. and Pattern Recognit., 2009. CVPR 2009. IEEE Conf. on*, pages 2044–2051. IEEE.

Lantagne, M., Parizeau, M., and Bergevin, R. (2003). Vip:

Vision tool for comparing images of people. In *Vis. Interface*, volume 2.

Lu, J. and Zhang, E. (2007). Gait recognition for human identification based on ica and fuzzy svm through multiple views fusion. *Pattern Recognit. Lett.*, 28(16):2401–2411.

Renò, V., Marani, R., D'Orazio, T., Stella, E., and Nitti, M. (2014). An adaptive parallel background model for high-throughput video appl. and smart cameras embedding. In *Proc. of the Int. Conf. on Distrib. Smart Cameras*, ICDSC '14, pages 30:1–30:6, New York, NY, USA. ACM.

Roy, A., Sural, S., and Mukherjee, J. (2012). A hierarchical method combining gait and phase of motion with spatiotemporal model for person re-identification. *Pattern Recognit. Lett.*, 33(14):1891–1901.

Saghafi, M. A., Hussain, A., Zaman, H. B., and Saad, M. H. M. (2014). Review of person re-identification techniques. *IET Comput. Vis.*, 8(6):455–474.

Spagnolo, P., Leo, M., D'Orazio, T., and Distante, A. (2004). Robust moving objects segmentation by background subtraction. In *The International Workshop on Image Analysis for Multimedia Interactive Services (WIAMIS)*.

Stauffer, C. and Grimson, W. E. L. (1999). Adaptive background mixture models for real-time tracking. In *Comput. Vis. and Pattern Recognit., 1999. IEEE Comput. Soc. Conf. on.*, volume 2. IEEE.

Wang, X., Doretto, G., Sebastian, T., Rittscher, J., and Tu, P. (2007). Shape and appearance context modeling. In *Comput. Vis., 2007. ICCV 2007. IEEE 11th Int. Conf. on*, pages 1–8. IEEE.

Yang, L. and Jin, R. (2006). Distance metric learning: A comprehensive survey. *Michigan State Universiy*, 2.

Zheng, W.-S., Gong, S., and Xiang, T. (2009). Associating groups of people. In *Proc. of the British Machine Vis. Conf.*, pages 23.1–23.11. BMVA Press. doi:10.5244/C.23.23.

Zivkovic, Z. (2004). Improved adaptive gaussian mixture model for background subtraction. In *Pattern Recognit., 2004. ICPR 2004. Proc. of the 17th Int. Conf. on*, volume 2, pages 28–31 Vol.2.